Schizophrenia Bulletin
doi:10.1093/schbul/sby011

Glutamate Dehydrogenase–Deficient Mice Display Schizophrenia-Like Behavioral Abnormalities and CA1-Specific Hippocampal Dysfunction

Sharon S. Lander[1], Usman Khan[2], Nicole Lewandowski[2], Darpan Chakraborty[1], Frank A. Provenzano[2], Susana Mingote[2,3], Sergiy Chornyy[1], Francesca Frigerio[4], Pierre Maechler[4], Hanoch Kaphzan[1], Scott A. Small[2], Stephen Rayport[2,3], and Inna Gaisler-Salomon[1,*]

[1]Department of Psychology or Neurobiology, University of Haifa, Haifa, Israel; [2]Department of Neurology or Psychiatry, Columbia University, New York, NY; [3]Department of Molecular Therapeutics, New York State Psychiatric Institute, New York, NY; [4]Department of Cell Physiology and Metabolism, Geneva University Medical Center, Geneva, Switzerland

*To whom correspondence should be addressed; 199 Abba Khoushi Ave, Haifa, Israel; tel: +972-4-8249674, fax +972-4-8240966, email igsalomon@psy.haifa.ac.il

Brain imaging has revealed that the CA1 subregion of the hippocampus is hyperactive in prodromal and diagnosed patients with schizophrenia (SCZ), and that glutamate is a driver of this hyperactivity. Strikingly, mice deficient in the glutamate synthetic enzyme glutaminase have CA1 hypoactivity and a SCZ-resilience profile, implicating glutamate-metabolizing enzymes. To address this further, we examined mice with a brain-wide deficit in the glutamate-metabolizing enzyme glutamate dehydrogenase (GDH), encoded by Glud1, which should lead to glutamate excess due to reduced glutamate metabolism in astrocytes. We found that Glud1-deficient mice have behavioral abnormalities in the 3 SCZ symptom domains, with increased baseline and amphetamine-induced hyperlocomotion as a positive symptom proxy, nest building and social preference as a negative symptom proxy, and reversal/extradimensional set shifting in the water T-maze and contextual fear conditioning as a cognitive symptom proxy. Neuroimaging of cerebral blood volume revealed hippocampal hyperactivity in CA1, which was associated with volume reduction. Parameters of hippocampal synaptic function revealed excess glutamate release and an elevated excitatory/inhibitory balance in CA1. Finally, in a direct clinical correlation using imaging-guided microarray, we found a significant SCZ-associated postmortem reduction in GLUD1 expression in CA1. These findings advance GLUD1 deficiency as a driver of excess hippocampal excitatory transmission and SCZ symptoms, and identify GDH as a target for glutamate modulation pharmacotherapy for SCZ. More broadly, these findings point to the likely involvement of alterations in glutamate metabolism in the pathophysiology of SCZ.

Key words: mouse model/CA1/fMRI/CBV/behavior/amphetamine-induced hyperactivity

Introduction

Alterations in glutamate signaling were first implicated in the neurobiology and symptomatology of schizophrenia (SCZ) with the observation of the psychotomimetic effects of phencyclidine and other NMDA glutamate receptor blockers.[1,2] Brain tissue studies have pointed to alterations in glutamate metabolism.[3] Many SCZ-associated genes converge at the glutamate synapse[4] and have been identified in large-scale genomic studies.[5]

Functional brain imaging has identified abnormalities in the hippocampal formation in SCZ, starting with the initial findings of an association of increased left parahippocampal activity with psychosis.[6] While decreased hippocampal activation has been seen in SCZ during semantic recall,[7] resting state studies have revealed hyperperfusion in the hippocampus[8] and subsequently in the left parahippocampal gyrus.[9] Hippocampal hyperactivity correlates across symptom domains,[10,11] is present in prodromal and first-episode patients,[12,13] and may stem from a disrupted excitatory/inhibitory balance.[14,15] Structural imaging has consistently identified hippocampal volume reductions in SCZ.[16,17]

The hippocampus is a heterogeneous structure, composed of uniquely connected subregions characterized by distinct molecular and functional profiles. The subregions are differentially affected in different disorders.[18] In SCZ, the hippocampal CA1 subregion appears to be most affected both structurally and functionally.[13,19,20] Recent longitudinal measures of cerebral blood volume (CBV), a variant of fMRI that allows for quantifiable and near-microscopic resolution of sub-regional vulnerability,[21,22] have shown that in SCZ hippocampal hypermetabolism occurs first in the CA1 subregion,[13,20] is related

to enhanced glutamate release, and correlates with tissue loss.[23] Evidence from animal models supports the role played by excitatory transmission, particularly in the hippocampus, in SCZ-related psychopathology.[24–28] While the contribution of postsynaptic glutamate receptors to SCZ psychopathology has been more extensively examined,[2,24,28] less is known about the involvement of alterations of enzymes involved in glutamate metabolism and homeostasis.

Mice deficient in the glutamate synthesizing enzyme glutaminase (*Gls1*) have decreased hippocampal activity, mainly in CA1, the inverse of the clinical imaging findings.[29] Ketamine-induced frontal cortical activation is also reduced. The mice respond less to the acute behavioral stimulating effects of amphetamine (AMPH), and also show diminished sensitization.[30] They show less AMPH-induced striatal dopamine release and antipsychotic drug-like potentiation of latent inhibition. These observations provide further support for the pivotal role of altered glutamatergic synaptic transmission in the pathophysiology of SCZ, and suggest that tempering glutamate release may provide a new therapeutic direction for the pharmacotherapy of SCZ. Whether decreased glutamate metabolism and increased glutamate would engender a SCZ-like profile has not been addressed.

Glutamate dehydrogenase 1 (GDH) is one of the major enzymes of glutamate metabolism.[31,32] It is an evolutionarily conserved mitochondrial enzyme that connects carbohydrate and glutamate metabolism.[33,34] In the CNS, GDH is mainly expressed in astrocytes,[35] where it catabolizes glutamate to alpha-ketoglutarate.[32] Interestingly, patients with mesial temporal lobe epilepsy, with SCZ-like psychotic symptoms and cognitive deficits, show a reduction of GDH activity and elevated glutamate in the hippocampus.[36] Postmortem SCZ studies reveal abnormal GDH in PFC and cerebellum although findings are inconsistent and confounded by variability in patient populations, measurement techniques, and treatment history.[37,38]

Here we have examined CNS-*Glud1*−/− mice with a brain-wide reduction in *Glud1*[39,40] in a battery of behavioral assays relevant to SCZ symptomatology and hippocampal function. We measured CBV to examine subregional activity and structural changes within the hippocampal formation. We assessed parameters of excitatory synaptic transmission and excitatory/inhibitory balance in the most affected hippocampal subregion, and associated alterations in gene expression as a measure of excitatory neuronal function. Finally, in a direct clinical correlation, we performed an imaging-guided postmortem microarray study to identify genes differentially expressed in affected vs. nonaffected hippocampal subregions of patients with SCZ. Our findings implicate GDH abnormalities in SCZ-related pathology and support the role played by glutamate-driven CA1 hyperactivity in the disease.

Methods

Full experimental procedures are described in the Supplemental Information.

CNS-Specific Glud1 Knockout Mice

Glud1$^{lox/lox}$ mice[41] were crossed with mice expressing Cre recombinase under the control of the nestin cis-regulatory sequence (B6.Cg-Tg Nes-Cre mice).[42] Heterozygous Nestin-Cre::*Glud1*+/− (CNS-*Glud1*+/−) mice were crossed to obtain homozygous Nestin-Cre::*Glud1*−/− (CNS-*Glud1*−/−), heterozygous CNS-*Glud1*+/−, and Nestin-Cre::*Glud1*+/+ (C-Cre+) control mice. Animals were maintained on a mixed C57BL/6J × 129/Sv genetic background. Behavioral, metabolic, physiological, and molecular experiments were performed in separate cohorts of mice. Experiments were performed in accordance with NIH guidelines under protocols approved by the IACUCs at the University of Haifa, NYS Psychiatric Institute and Columbia University.

Behavioral Studies

Adult CNS-*Glud1*−/−, CNS-*Glud1*+/−, and C-Cre+ mice (PND 60–95) were tested in 3 cohorts. The first cohort included male and female mice, tested for deficits in nesting behavior, baseline locomotor activity, social preference, water T-maze, and d-AMPH-induced hyperactivity. As previously described,[43] tests were performed on consecutive days, except for a 7-day rest following the water T-maze. No significant sex differences were found; data from male and female mice were combined. The second and third cohort included male mice tested in trace and foreground contextual fear conditioning, respectively.[44] Trials were recorded and analyzed using FreezeFrame (Actimetrics, Evanston, IL) or Ethovision XT9.0 software (Noldus Information Technology, Leeburh, VA).

Neuroimaging

Image Acquisition. Mice were anesthetized with a mixture of 30% O_2, 70% N_2, and isoflurane (3% volume for induction; 1.1–1.5% for maintenance at 1 L/min, via a nose cone). Images were acquired with a Bruker AVANCE 400WB spectrometer outfitted with an 89-mm bore, 9.4-T vertical Bruker magnet (Oxford Instruments Ltd., United Kingdom), a 30-mm inner-diameter birdcage radio frequency coil, and a shielded gradient system (100 G/cm). Baseline images were acquired; then the contrast agent gadolinium was administered[45] (10 mmol/kg intraperitoneally) and after 37.5 minutes further images acquired. T2-weighted images were acquired with a fast-spin echo acquisition (time to repeat, 2,000 ms; time to echo, 70 ms; rapid acquisition and relaxation enhancement factor, 16; in plane resolution, 86 μm; slice thickness, 500 μm).

CCBV Maps. High-resolution mouse CBV maps were generated as previously described.[45,46] Briefly, changes

were mapped in the transverse relaxation time (ΔR_2) of the T2-weighted protocol induced by gadolinium injection. CBV was derived by normalizing ΔR_2 to the mean ΔR_2 signal present in the internal jugular vein, as delineated by a blinded rater.

Voxel-Based Analysis of CBV. As previously described in greater detail,[47] re- and post-gadolinium structural images were co-registered for each mouse to generate an animal-specific median image using a robust, inverse-consistent linear registration.[48]

Hippocampal Structure and Morphometry. Rodent morphometry was conducted in a separate voxel-based framework as previously described.[23,49]

Glutamate Measurements

Glutamine and glutamate levels were measured in the right hippocampus by liquid chromatography-tandem mass spectrometry (LC/MS-MS) using the SCIEX API4000 (Applied Biosystems), as previously described.[50]

Brain Slice Electrophysiology

Electrophysiology was performed in sagittal slices. Standard procedures were used to assess miniature excitatory and inhibitory postsynaptic currents (mEPSCs and mIPSCs, respectively) as well as evoked EPSCs and IPSCs in CA1 pyramidal neurons with stimulation of Schaffer collaterals (see SI). Cellular excitability was assessed as previously described.

Gene Expression

mRNA gene expression levels in right CA1 and CA3 and in mPFC were determined by real-time quantitative PCR (qRT-PCR) as previously described.[43] Expression of markers of excitatory neurotransmission was analyzed; see SI for full list of genes and primer sequences. Statistical analyses were performed on ΔCT, that is, intensity values for genes of interest normalized to Hypoxanthine Guanine Phosphoribosyltransferase (HPRT). Fold change was calculated as $2^{-\Delta\Delta CT}$ relative to the C-Cre+ group.

Postmortem Gene Expression Profiling

Brain samples from 10 patients with SCZ (mean age = 51 years; 3 female) and 9 age-matched controls (mean age = 49 years, 1 female) were obtained from the Harvard Brain Tissue Resource Center (HBTRC). All tissue diagnoses were confirmed by retrospective review of clinical records and a comprehensive neuropathological examination (https://hbtrc.mclean.harvard.edu/investigators). Hippocampal subfield dissection was performed at the New York Brain Bank (NYBB) by a neuropathologist who identified and sectioned the CA1 subregion and the relatively unaffected[51] entorhinal cortex (EC) using strict anatomical criteria following NYBB procedures. Profiling transcripts from both a region targeted by a disease and from a within-brain neighboring control region has proven effective in addressing analytic challenges inherent to gene-expression studies.[52]

Total RNA was extracted from each of the 40 tissue samples, and fragmented cRNA was prepared following the Affymetrix eukaryotic target preparation protocol found in the GeneChip Expression Analysis Technical Manual (http://www.affymetrix.com/support/technical/manual/expression_manual.affx). In the Gene Chip Analysis Facility of Columbia University, HG-U133A 2.0 microarrays (GeneChip, Affymetrix) were hybridized with fragmented cRNA, washed and stained on a fluidics station, and scanned using a laser confocal microscope. Microarrays were analyzed with Affymetrix Microarray Suite v5.0 and GeneSpring v5.0.3 (Silicon Genetics, Redwood City, CA) software, and scaled to a value of 500.

Statistical analyses are detailed in SI.

Results

CNS-Glud1−/− Mice Show SCZ-Like Behavior

We used mice with a homozygous (CNS-*Glud1*−/−) or heterozygous (CNS-*Glud1*+/−) deletion of *Glud1* restricted to the CNS by Nestin-cre, and Nestin-cre (C-Cre+) mice as controls. We tested the mice in behavioral assays designed to detect deficits spanning the 3 major domains of SCZ symptomatology. To assess positive symptom-like behaviors, we measured baseline and AMPH-induced hyperlocomotion, as correlates of the hyperdopaminergic state that characterizes psychosis.[53] To assess negative symptom-like behaviors, we measured nest building deficits, mimicking anhedonia and self-neglect,[54] and social preference.[55] As a cognitive symptom proxy, we measured reversal/extradimensional set shifting in the water T-maze.[43,56] Except for the open field, where males of all genotypes spent significantly less time in the *anxiogenic* center than females (mean ± SEM: females 255.07 ± 24.44 s, males 322.87 ± 19.84 s, $F(1,51) = 4.719$, $P < .05$), no sex differences nor sex × genotype interactions were found in any of the assays; we therefore combined data from male and female mice in subsequent analyses. In order to minimize testing-induced effects that could mask genotypic differences, tests were conducted in the following order: nesting, baseline locomotor activity, social preference, water T-maze, AMPH-induced hyperlocomotion. Results are reported in the order conducted.

CNS-*Glud1*−/− mice showed inferior nest-building (figure 1A) and hyperlocomotion in the open field (figure 1B), where there were no genotypic differences in avoidance of the *anxiogenic* center of the open field (not shown). To evaluate social dysfunction, we tested

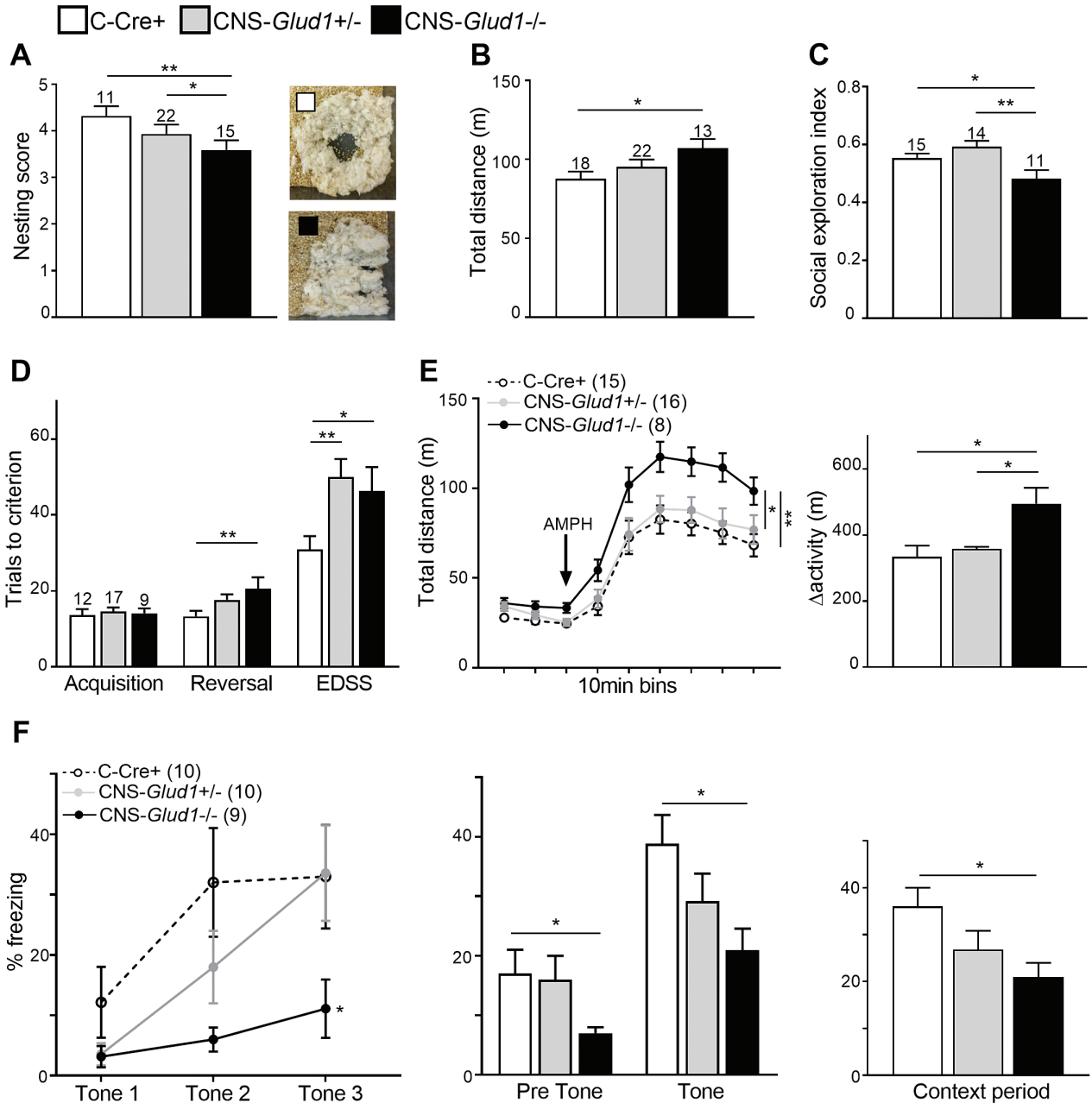

Fig. 1. CNS-*Glud1*−/− mice display SCZ-like behavioral deficits. (A) CNS-*Glud1*−/− mice display low nesting scores (F[2,42] = 3.425, $P < .05$). *Right*: Representative images of C-Cre+ (*top*) and CNS-*Glud1*−/− (*bottom*) nests, and increased locomotor activity in the open field (B, F(2,50) = 3.275, $P < .05$). (C) CNS-*Glud1*−/− mice also show decreased social exploration (F[2,37] = 6.240, $P < .01$), with no differences in the number of entries into all chambers (F[1,25] = 1.250, $P > .1$). (D) In the water T-maze, mice show a genotype-dependent increase in trials to criterion with each stage (stage, Huynh-Feldt correction F(1.361,47.649) = 61.402, $P < .0001$; genotype F(2,35) = 9.627, $P < .0001$, stage × genotype interaction Huynh-Feldt correction F(2.723,47.649)=3.015, $P < .05$). CNS-*Glud1*−/− mice require more trials to reach criterion in reversal (F[2,35] = 6.090, $P < .01$). Both CNS-*Glud1*−/− and CNS-*Glud1*+/− require more trials to criterion in the extra-dimensional set-shifting (EDSS) stage (F[2,35] = 4.875, $P < .05$). (E) *Left*, *CNS-Glud1*−/− mice show enhanced baseline (F[2,36] = 3.756, $P < .05$) and AMPH (2 mg/kg)-induced hyperlocomotion (genotype, F[8,288] = 117.575, $P < .0001$, time × genotype interaction F[16,288] = 1.716, $P < .05$; 10-min bins), as well as higher Δactivity (AMPH/baseline locomotion; *Right*, F[2,36] = 3.479, $P < .05$). (F) *Left*, in trace fear conditioning, all genotypes show a time-dependent increase in freezing during tone presentation (acquisition, F[2,52] =10.683 $P < .001$). CNS-*Glud1*−/− mice show an attenuated increase in freezing during acquisition (F[2,26] = 4.58, $P < .05$). *Center*, all genotypes show an increase in freezing after tone presentation during the Tone Test (F[1,26] =72.556, $P < .001$). CNS-*Glud1*−/− mice show attenuated freezing throughout the Tone Test (F[2,26] = 3.667, $P < .05$). *Right*, CNS-*Glud1*−/− display attenuated freezing during the Context Test (F[2,26] = 4.371, $P < .05$). With the exception of the EDSS stage of the water T-maze, CNS-*Glud1*+/− mice did not differ from controls. Data are presented as mean ± SEM. *$P < .05$, **$P < .01$.

preference towards social vs inanimate novel stimuli and found a lower social exploration index in CNS-*Glud1*−/− mice (figure 1C), with no differences in measures of total exploration scores or the total number of entries into all chambers (not shown). In the 3-stage water T-maze task, we found a genotype-dependent increase in the number of trials to criterion with each consecutive stage (figure 1D). Separate analysis of trials to criterion in each stage revealed no genotypic differences in spatial acquisition, and a gene-dose effect in the reversal and extra-dimensional set-shifting (EDSS) stages: while CNS-*Glud1*−/− mice were impaired in both stages, CNS-*Glud1*+/− mice were impaired in the more challenging (EDSS) stage. Finally, we examined baseline and AMPH-induced hyperlocomotion in CNS-*Glud1*−/− mice (figure 1E, left). Analysis of Δactivity (response to AMPH relative to baseline) revealed that hyperlocomotion following AMPH administration was increased in CNS-*Glud1*−/− mice (figure 1E, right). Again, no genotypic differences were observed in the time spent in the center of the open field. Overall, these findings identify behavioral abnormalities in correlates of positive, negative, and cognitive SCZ symptom domains in CNS-*Glud1*+/− mice.

In a separate cohort of mice, we tested deficits in trace fear conditioning, a task that relies on intact function of the amygdala and hippocampus and is sensitive to glutamatergic manipulations.[44,57] Pre-tone freezing did not differ between C-Cre+ and CNS-*Glud1*−/− mice. CNS-*Glud1*−/− mice displayed deficits in acquiring trace fear and impaired retrieval of cued and contextual information (figure 1F). In order to investigate hippocampal dependent contextual learning separately from cued learning, we assessed foreground fear conditioning in C-Cre+ and CNS-*Glud1*−/− mice. We found no differences in pre-shock (baseline) freezing levels during Acquisition (not shown), but impaired retrieval of contextual information in CNS-*Glud1*−/− mice (C-Cre+, 55.2 ± 8.3; CNS-*Glud1*−/−, 31.47 ± 5.08). Notably, with the exception of the EDSS stage of the water T-maze, no abnormalities were found in heterozygous CNS-*Glud1*+/− mice.

SCZ-Like Functional and Structural CA1 Abnormalities

Because behavioral tests point to SCZ-like phenotypes and hippocampal dysfunction in CNS-*Glud1*−/− mice, we asked whether they phenocopy the neuroimaging profile of hippocampal dysfunction observed in the disease. We used the same steady-state CBV-fMRI approach applied to patients.[23] A voxel-based statistical analysis of the hippocampus was conducted comparing CNS-*Glud1*−/− to C-Cre+ mice. CNS-*Glud1*−/− mice had significant increases in CBV, primarily in the intermediate to dorsal CA1, which partially extended into other hippocampal regions. The effect was more prominent in the right hemisphere (figures 2A and 2C). To assess associated structural alterations, we performed voxel-based morphometry, as previously described,[23] in the pre-gadolinium scans. CNS-*Glud1*−/− mice, compared with C-Cre+ controls, showed volume reduction in the anatomical vicinity of CBV abnormalities in CA1. Volume reductions were also more prominent in the right hemisphere (figures 2B and 2C).

To address the contribution of increased glutamatergic transmission, we asked whether glutamate levels were increased in the hippocampus of CNS-*Glud1*−/− mice. Using MS to measure glutamate in CNS-*Glud1*−/− mice (n = 12) and C-Cre+ controls (n = 14), we found a 39% increase in glutamate in the right hippocampus of CNS-*Glud1*−/− mice (7.5842 ± 0.27907 µmol/g) compared with C-Cre+ controls (5.4429 ± 0.19486 µmol/g; $F(1,24) = 41.362$; $P < .00001$, not shown). No differences in glutamine levels were found.

Abnormal Glutamatergic Transmission in CA1

To determine whether glutamate synaptic transmission was affected, we measured gene expression for key mediators of glutamate synthesis or release (vesicular glutamate transporter 1 [vGlut1], Complexin 2 [Cx2], glutaminase [Gls]), glutamate receptor subunits (NMDA subunit types 1 and 2A [NR1, NR2A] and AMPA receptor subunit types 1 and 2 [GluA1, GluA2]), and glutamate reuptake (excitatory amino acid transporters 1 [EAAT1] and 2 [EAAT2]). In the right intermediate hippocampal CA1 region, we found increased mRNA expression of Cx2, NR2A, GluA2, EAAT1, and EAAT2 (figure 3A), but no differences in CA3 (figure 3B). In the mPFC, we found increased expression of the neuronal excitatory marker Cx2 but not in other genes (figure 3C). Taken together, these findings identify abnormalities in glutamate neurotransmission dynamics mostly in CA1. Analysis of regional differences in NMDA receptor subunit expression in control C-Cre+ mice revealed a significant 7.5-fold increase in NR2A mRNA in CA1 compared with mPFC ($F[1,11] = 36.112$, $P < .001$); no differences in NR1 expression were observed.

To measure glutamatergic synaptic transmission directly, we examined spontaneous input activity in CA1 pyramidal neurons in the right intermediate-to-dorsal hippocampal CA1 region of C-Cre+ and CNS-*Glud1*−/− mice (figures 4A and 4B, left panels). There was a rightward shift in mEPSC amplitude distribution in CNS-*Glud1*−/− mice and a corresponding increase in the average mEPSC amplitude (figure 4A, center). No alterations were observed in the cumulative probability of inter-event intervals or in average event frequency (figure 4A, right). In contrast, mIPSCs in CNS-*Glud1*−/− mice were altered in both amplitude and frequency; there was a significant rightward shift in the amplitude distribution and an increase in amplitude (figure 4B, center). The mIPSC distribution of interevent intervals was

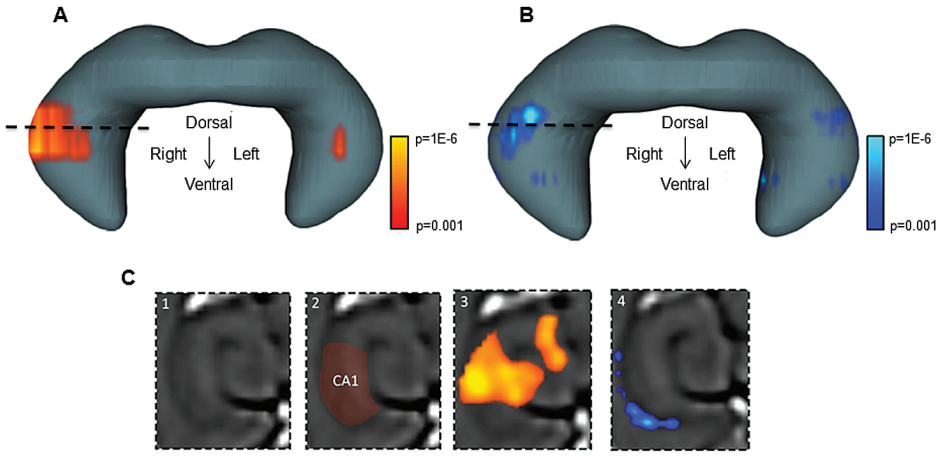

Fig. 2. Functional and structural deficits in the hippocampus of CNS-*Glud1*−/− mice. (A) A voxel-based analysis of hippocampal cerebral blood volume (CBV) maps is shown superimposed on a 3D rendering of the entire hippocampus. CNS-*Glud1*−/− mice show a selective pattern of CBV increases in CA1, compared with C-Cre+ mice ($t_{(19)} = 4.44$, $P < .001$). Voxels with P value ≥.001 are coded with warm colors (red to yellow). (B) A voxel-based morphometric analysis of the hippocampus is superimposed on the 3D rendering of the hippocampus. CNS-*Glud1*−/− mice show a selective pattern of relative atrophy in the vicinity of the CBV increases ($t_{(9)} = 3.95$). Voxels with a P value ≥.001 are coded with cool colors (royal blue to aqua blue). (C) A transaxial structural image is shown, at the level of the stippled lines in panels A and B. The CA1 region is indicated by red shading (C2). Statistical maps of increased CBV (C3) and decreased morphometry (C4) overlap the CA1 region. *n*'s: C-Cre+ 10, CNS-*Glud1*−/− 10).

right-shifted and the average mIPSC frequency was lower (figure 4B, right).

Examining Schaffer collateral evoked activity in CA1 pyramidal neurons, we found an increase in the average excitatory to inhibitory (E/I) ratio in CNS-*Glud1*−/− mice (figure 4C). Changes in the E/I balance could be related to abnormal NMDA- or AMPA-mediated signaling. In CNS-*Glud1*−/− mice, the AMPA/NMDA ratio was increased (figure 4D). An assessment of passive membrane properties of CA1 pyramidal cells showed that the resting membrane potential was comparable in both genotypes (figure 4E), but input resistance was increased in CNS-*Glud1*−/− mice (figure 4F), perhaps reflecting a reduction in chloride conductance in line with reduced mIPSC frequency. Active membrane properties, including action potential (AP) threshold, amplitude, and after-hyperpolarization, were unaltered (figure S1). Half-width was increased in CNS-*Glud1*−/− mice (figure S1C). The firing-input (F-I) curve was enhanced (figure 4G). Taken together, these findings provide further support for glutamate-driven hyperactivity in the CA1 of CNS-*Glud1*−/− mice.

SCZ-Associated Reduction in GLUD1 mRNA Levels

Guided by the finding that CA1 is selectively affected in CNS-*Glud1*−/− mice, together with the associated SCZ-like behavioral and metabolic abnormalities, we profiled gene expression in postmortem tissue harvested from CA1 and from the less affected neighboring EC of patients with SCZ and age-matched controls. Nineteen transcripts that showed a significant group × region interaction at a $P < .005$ level were identified, including *GLUD1*, which was significantly downregulated ($P < .0001$; SI table 1).

Discussion

CNS-specific abrogation of *Glud1*, encoding the principal glutamate-metabolizing enzyme GDH, leads to behavioral deficits in the 3 SCZ symptom domains. In line with neuroimaging findings in prodromal and diagnosed patients with SCZ, *Glud1*-deficient mice display CA1 hyperactivity and associated volume reductions. Further investigation of hippocampal function reveals excess glutamate and increased glutamatergic synaptic transmission. In a clinical correlation, a postmortem imaging-guided microarray study identified a significant SCZ-associated reduction in *GLUD1* expression in CA1, supporting CNS-*Glud1*−/− mice as a glutamate-based mouse model uniquely relevant to the pathophysiology of SCZ. Together with the postmortem results, our findings implicate reductions in *GLUD1* in the hippocampus as a pathogenic mechanism in SCZ.

CNS-*Glud1*−/− mice exhibit behavioral alterations that align with SCZ symptomatology,[23,54–56] including enhanced sensitivity to the psychotomimetic drug AMPH, diminished preference for social stimuli, self-neglect, and compromised cognitive function. The behavioral profile of CNS-*Glud1*−/− mice aligns also with hippocampal dysfunction, evidenced in deficient nest-building[58] and contextual fear learning.[59] Interestingly, heterozygous CNS-*Glud1*−/+ mice were normal in all behavioral assays except for the set-shifting component

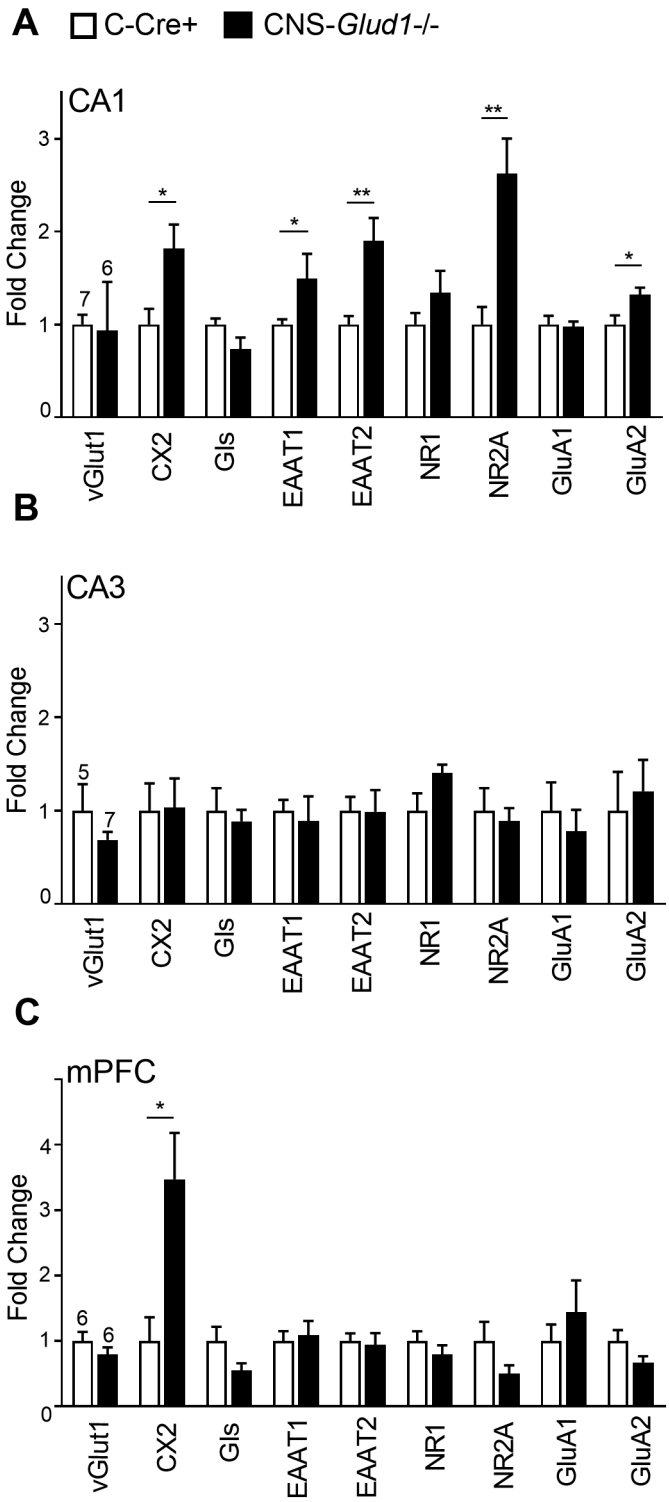

Fig. 3. CNS-*Glud1*−/− mice show increased expression of excitatory markers in CA1. (A) In the right CA1, CNS-*Glud1*−/− mice show increased expression of excitatory markers Cx2 (F[1,11] = 7.136; $P < .05$), NR2A (F[1,11] = 9.568; $P < .05$), GluA2 [F[1,11] = 5.342; $P < .05$), EAAT1 (F[1,11] = 5.049; $P < .05$), and EAAT2 (F[1,11] = 17.082; $P < .01$); *n*'s: C-Cre+ 7 (CNS-*Glud1*−/− 6). (B) In CA3, no genotypic differences were found (*n*'s: C-Cre+ 7, CNS-*Glud1*−/− 6). (C) In mPFC, CNS-*Glud1*−/− mice showed increased expression of Cx2 (F[1,10] = 9.078; $P < .05$, *n*'s: C-Cre+ 6, CNS-*Glud1*−/− 6). Data are presented as mean fold change ± SEM. *$P < .05$, **$P < .01$.

of the water T-maze. Possibly, more demanding cognitive tasks reveal more subtle deficits.

Metabolic imaging of CNS-*Glud1*−/− mice reveals a pattern of hyperactivity predominantly in the CA1 region, generally consistent with the pattern observed in patients, except that the defect is right predominant in mice and left predominant in patients.[13,23] In patients, rCBV in the left hippocampus was differentially correlated with positive symptoms, specifically with measures of delusions,[13] whereas in mice we also observed phenotypes that mimic negative and cognitive symptoms. The hemispheric predominance of the CBV effect may depend on the specific subset of patients studied, and the prevalence of SCZ-associated symptoms. Strikingly, the increase in metabolism overlapped with volume reductions in CA1, not only in being greatest in the intermediate hippocampus in CA1, but also in correlating in right-sided predominance.

CNS-*Glud1*−/− mice show hippocampal glutamate abnormalities, previously observed in patients with SCZ and in animal models of the disorder.[23] Specifically, our data point to enhanced glutamate levels, abnormally elevated transcript levels of glutamate markers and higher excitability of CA1 pyramidal neurons. These findings align with human studies showing enhanced glutamate levels and abnormal expression of glutamate markers in SCZ.[60–62] Our findings are also consistent with animal studies that show a positive correlation between hippocampal glutamate and SCZ-like phenotypes, and point to glial dysfunction as a key player in maintaining glutamate homeostasis.[23,29,63–65]

While mEPSC and mIPSC amplitude are increased in CA1 slices from CNS-*Glud1*−/− mice, only mIPSC frequency was decreased. Thus, a homeostatic balance in GABA transmission is maintained, while pyramidal neuron firing is abnormally increased.[66] Elevated intrinsic excitability is also observed in CNS-*Glud1*−/− mice, possibly affecting synaptic potentiation.[67]. Similar abnormalities in passive membrane properties, generally pointing to increased pyramidal neuron firing and an elevated E/I balance in CA1, have been reported in mouse models of neurodevelopmental disorders, including SCZ[68].

Reduced *Glud1* expression would be expected to result in increased glutamate, as GDH is predominantly expressed in astrocytes where its role is catabolic.[32,35] However, a previous study in CNS-*Glud1*−/− mice revealed no change in brain glutamate levels,[39] possibly because Nestin-Cre-expressing mice (which display reduced body weight and altered fear conditioning)[40,69] were not included as controls.[40,70] Moreover, glutamate levels were assessed in the entire brain, and not in the hippocampus as in this study.

Our data point to some selectivity in the effects of Nestin-Cre driven *Glud1* deletion, so that the CA1 displays disturbed glutamate dynamics, while other regions are spared. Interestingly, neuron-specific *Glud1* overexpression also has a particularly pronounced impact

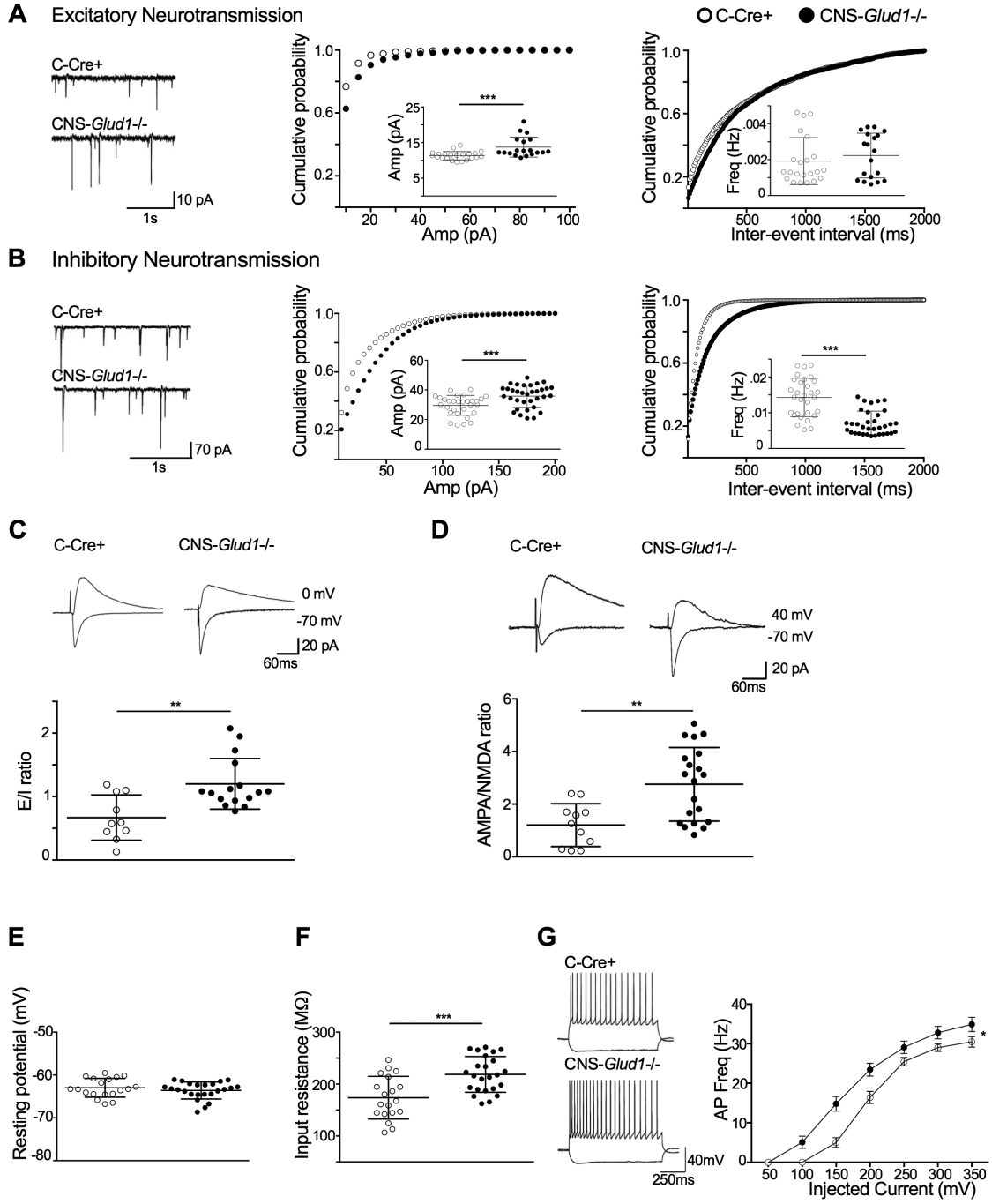

Fig. 4. Altered excitatory and inhibitory transmission in CA1. (A) Excitatory synaptic activity. *Left*, representative traces of whole-cell voltage clamp recordings of mEPSCs. *Center*, rightward shift in the cumulative frequency distribution of mEPSC amplitude ($P < .01$) and an increase in the average amplitude in CNS-*Glud1*−/− mice (inset, $t_{(39)} = 3.65$, $P < .001$). *Right*, no genotypic differences in the interevent interval. (B) Inhibitory synaptic activity. *Left*, representative traces of whole-cell voltage clamp recordings of mIPSCs. *Center*, CNS-*Glud1*−/− mice show a rightward shift in the cumulative frequency distribution of mIPSC amplitude ($P < .01$) and an increase in the average amplitude (inset, $t_{(62)}$=3.474, $P < .001$). *Right*, a decrease in cumulative frequency of interevent intervals ($P < .0001$) and a lower average in CNS-*Glud1*−/− mice (inset, $t_{(62)} = 6.52$, $P < .001$). (C) CNS-*Glud1*−/− mice show elevated mean *E*/*I* ratios ($t_{(24)} = 3.43$, $P < .005$). *Top*, sample traces for evoked responses, with voltage clamped at −70 mV for eEPSCs and 0 mV for eIPSCs. (D) CNS-*Glud1*−/− mice show an elevated mean AMPA/NMDA ratio ($t_{(29)} = 3.35$, $P < .01$). Bicuculline (50 μM, Tocris, Ellisville, MI) was added to the bath to block $GABA_A$ receptors. *Top*, sample traces, with voltage clamped at +40 mV for NMDA and −70 mV for AMPA. (E) Mean resting membrane potential, measured under current clamp, is unchanged. (F) Average input resistance is higher ($t_{(42)} = 3.88$, $P < .001$). (G) CNS-*Glud1*−/− mice show a leftward shift in the firing index and higher firing frequency (group × current steps intensity interaction: Huynh-Feldt correction $F(3.311, 139.065) = 5.467$, $P < .001$). *Left*, representative traces display the response of CA1 pyramidal cells with a 1-s long current injection of −100 pA and +150 pA. *n*'s: C-Cre+ 22, CNS-*Glud1*−/− 19. Data are presented as mean ± SEM. *$P < .05$, **$P < .01$, ***$P < .001$.

on CA1 physiology and morphology.[71] The molecular determinants of selective CA1 vulnerability to abnormal *Glud1* expression and glutamate levels are not known, but could be related to high expression of NMDA receptors or altered receptor subunit distribution in this region, as shown in this study and in previous investigations.[72]

Taken together, these findings lend support for the involvement of the glutamatergic system, particularly during the early hypermetabolic stage of disease,[18] in the pathobiology of SCZ[2,73] and implicate the pathway of enzymes that regulate the catabolism and metabolism of brain glutamate.[74] Further studies should examine this pathway as a regulator of hippocampal hyperactivity, and delineate the genetic and environmental factors that affect it. Better understanding of hippocampal glutamate dynamics is imperative for providing insight into mechanisms underlying SCZ symptoms, and for the development of novel treatment targets.

Supplementary Material

Supplementary material is available at *Schizophrenia Bulletin* online.

Funding

This study was supported by an Israel Science Foundation grant 484/10 to IGS, a US-Israel Binational Science Foundation grant 2009301 (to Drs Gaisler-Salomon, Rayport, and Small), Israel Science Foundation grant 287/15 (to Dr. Kaphzan), a Columbia University RISE award (to S.R.), and National Institutes of Health R01 MH093398 (to Dr. Small).

Acknowledgments

We thank Celia Gellman and Kenneth Hess for mouse imaging technical assistance, Matt I. Gross (Calithera Biosciences) for amino acid determinations, and Sophia E. Gorham for preliminary gene expression studies.
Conflict of Interest: The authors declare no conflicts of interest.

References

1. Malhotra AK, Pinals DA, Adler CM, et al. Ketamine-induced exacerbation of psychotic symptoms and cognitive impairment in neuroleptic-free schizophrenics. *Neuropsychopharmacology*. 1997;17:141–150.
2. Moghaddam B, Javitt D. From revolution to evolution: the glutamate hypothesis of schizophrenia and its implication for treatment. *Neuropsychopharmacology*. 2012;37:4–15.
3. Hu W, MacDonald ML, Elswick DE, Sweet RA. The glutamate hypothesis of schizophrenia: evidence from human brain tissue studies. *Ann N Y Acad Sci*. 2015;1338:38–57.
4. Harrison PJ, Weinberger DR. Schizophrenia genes, gene expression, and neuropathology: on the matter of their convergence. *Mol Psychiatry*. 2005;10:40–68; image 5.
5. Schizophrenia Working Group of the Psychiatric Genomics C. Biological insights from 108 schizophrenia-associated genetic loci. *Nature*. 2014;511:421–427.
6. Liddle PF, Friston KJ, Frith CD, Hirsch SR, Jones T, Frackowiak RS. Patterns of cerebral blood flow in schizophrenia. *Br J Psychiatry*. 1992;160:179–186.
7. Heckers S, Rauch SL, Goff D, et al. Impaired recruitment of the hippocampus during conscious recollection in schizophrenia. *Nat Neurosci*. 1998;1:318–323.
8. Medoff DR, Holcomb HH, Lahti AC, Tamminga CA. Probing the human hippocampus using rCBF: contrasts in schizophrenia. *Hippocampus*. 2001;11:543–550.
9. Malaspina D, Harkavy-Friedman J, Corcoran C, et al. Resting neural activity distinguishes subgroups of schizophrenia patients. *Biol Psychiatry*. 2004;56:931–937.
10. Tamminga CA, Stan AD, Wagner AD. The hippocampal formation in schizophrenia. *Am J Psychiatry*. 2010;167:1178–1193.
11. Tregellas JR, Smucny J, Harris JG, et al. Intrinsic hippocampal activity as a biomarker for cognition and symptoms in schizophrenia. *Am J Psychiatry*. 2014;171:549–556.
12. Allen P, Chaddock CA, Egerton A, et al. Resting hyperperfusion of the hippocampus, midbrain, and basal ganglia in people at high risk for psychosis. *Am J Psychiatry*. 2016;173:392–399.
13. Schobel SA, Lewandowski NM, Corcoran CM, et al. Differential targeting of the CA1 subfield of the hippocampal formation by schizophrenia and related psychotic disorders. *Arch Gen Psychiatry*. 2009;66:938–946.
14. Benes FM, Kwok EW, Vincent SL, Todtenkopf MS. A reduction of nonpyramidal cells in sector CA2 of schizophrenics and manic depressives. *Biol Psychiatry*. 1998;44:88–97.
15. Uhlhaas PJ. Dysconnectivity, large-scale networks and neuronal dynamics in schizophrenia. *Curr Opin Neurobiol*. 2013;23:283–290.
16. Adriano F, Caltagirone C, Spalletta G. Hippocampal volume reduction in first-episode and chronic schizophrenia: a review and meta-analysis. *Neuroscientist*. 2012;18:180–200.
17. Kraguljac NV, White DM, Reid MA, Lahti AC. Increased hippocampal glutamate and volumetric deficits in unmedicated patients with schizophrenia. *JAMA Psychiatry*. 2013;70:1294–1302.
18. Small SA. Isolating pathogenic mechanisms embedded within the hippocampal circuit through regional vulnerability. *Neuron*. 2014;84:32–39.
19. Narr KL, Thompson PM, Szeszko P, et al. Regional specificity of hippocampal volume reductions in first-episode schizophrenia. *Neuroimage*. 2004;21:1563–1575.
20. Talati P, Rane S, Kose S, et al. Increased hippocampal CA1 cerebral blood volume in schizophrenia. *Neuroimage Clin*. 2014;5:359–364.
21. Lin W, Celik A, Paczynski RP. Regional cerebral blood volume: a comparison of the dynamic imaging and the steady state methods. *J Magn Reson Imaging*. 1999;9:44–52.
22. Small SA, Wu EX, Bartsch D, et al. Imaging physiologic dysfunction of individual hippocampal subregions in humans and genetically modified mice. *Neuron*. 2000;28:653–664.
23. Schobel SA, Chaudhury NH, Khan UA, et al. Imaging patients with psychosis and a mouse model establishes a

spreading pattern of hippocampal dysfunction and implicates glutamate as a driver. *Neuron*. 2013;78:81–93.
24. Fradley RL, O'Meara GF, Newman RJ, Andrieux A, Job D, Reynolds DS. STOP knockout and NMDA NR1 hypomorphic mice exhibit deficits in sensorimotor gating. *Behav Brain Res*. 2005;163:257–264.
25. Lodge DJ, Grace AA. Aberrant hippocampal activity underlies the dopamine dysregulation in an animal model of schizophrenia. *J Neurosci*. 2007;27:11424–11430.
26. Lodge DJ, Grace AA. Hippocampal dysfunction and disruption of dopamine system regulation in an animal model of schizophrenia. *Neurotox Res*. 2008;14:97–104.
27. Moghaddam B, Jackson ME. Glutamatergic animal models of schizophrenia. *Ann N Y Acad Sci*. 2003;1003:131–137.
28. Mohn AR, Gainetdinov RR, Caron MG, Koller BH. Mice with reduced NMDA receptor expression display behaviors related to schizophrenia. *Cell*. 1999;98:427–436.
29. Gaisler-Salomon I, Miller GM, Chuhma N, et al. Glutaminase-deficient mice display hippocampal hypoactivity, insensitivity to pro-psychotic drugs and potentiated latent inhibition: relevance to schizophrenia. *Neuropsychopharmacology*. 2009;34:2305–2322.
30. Mingote S, Chuhma N, Kalmbach A, et al. Dopamine neuron dependent behaviors mediated by glutamate cotransmission. *Elife*. 2017;6. doi: 10.7554/eLife.27566.
31. Plaitakis A, Zaganas I. Regulation of human glutamate dehydrogenases: implications for glutamate, ammonia and energy metabolism in brain. *J Neurosci Res*. 2001;66:899–908.
32. Spanaki C, Kotzamani D, Petraki Z, Drakos E, Plaitakis A. Heterogeneous cellular distribution of glutamate dehydrogenase in brain and in non-neural tissues. *Neurochem Res*. 2014;39:500–515.
33. Hucho F, Rasched I, Sund H. Studies of glutamate dehydrogenase: analysis of functional areas and functional groups. *Eur J Biochem*. 1975;52:221–230.
34. Michaelis EK, Wang X, Pal R, et al. Neuronal Glud1 (glutamate dehydrogenase 1) over-expressing mice: increased glutamate formation and synaptic release, loss of synaptic activity, and adaptive changes in genomic expression. *Neurochem Int*. 2011;59:473–481.
35. Aoki C, Milner TA, Sheu KF, Blass JP, Pickel VM. Regional distribution of astrocytes with intense immunoreactivity for glutamate dehydrogenase in rat brain: implications for neuron-glia interactions in glutamate transmission. *J Neurosci*. 1987;7:2214–2231.
36. Malthankar-Phatak GH, de Lanerolle N, Eid T, et al. Differential glutamate dehydrogenase (GDH) activity profile in patients with temporal lobe epilepsy. *Epilepsia*. 2006;47:1292–1299.
37. Burbaeva GSh, Boksha IS, Tereshkina EB, et al. Systemic neurochemical alterations in schizophrenic brain: glutamate metabolism in focus. *Neurochem Res*. 2007;32:1434–1444.
38. Gluck MR, Thomas RG, Davis KL, Haroutunian V. Implications for altered glutamate and GABA metabolism in the dorsolateral prefrontal cortex of aged schizophrenic patients. *Am J Psychiatry*. 2002;159:1165–1173.
39. Frigerio F, Karaca M, De Roo M, et al. Deletion of glutamate dehydrogenase 1 (Glud1) in the central nervous system affects glutamate handling without altering synaptic transmission. *J Neurochem*. 2012;123:342–348.
40. Karaca M, Maechler P. Development of mice with brain-specific deletion of floxed glud1 (glutamate dehydrogenase 1) using cre recombinase driven by the nestin promoter. *Neurochem Res*. 2014;39:456–459.
41. Carobbio S, Frigerio F, Rubi B, et al. Deletion of glutamate dehydrogenase in beta-cells abolishes part of the insulin secretory response not required for glucose homeostasis. *J Biol Chem*. 2009;284:921–929.
42. Tronche F, Kellendonk C, Kretz O, et al. Disruption of the glucocorticoid receptor gene in the nervous system results in reduced anxiety. *Nat Genet*. 1999;23:99–103.
43. Lander SS, Linder-Shacham D, Gaisler-Salomon I. Differential effects of social isolation in adolescent and adult mice on behavior and cortical gene expression. *Behav Brain Res*. 2017;316:245–254.
44. Hazan L, Gaisler-Salomon I. Glutaminase1 heterozygous mice show enhanced trace fear conditioning and Arc/Arg3.1 expression in hippocampus and cingulate cortex. *Eur Neuropsychopharmacol*. 2014;24:1916–1924.
45. Moreno H, Hua F, Brown T, Small S. Longitudinal mapping of mouse cerebral blood volume with MRI. *NMR Biomed*. 2006;19:535–543.
46. Moreno H, Wu WE, Lee T, et al. Imaging the Abeta-related neurotoxicity of Alzheimer disease. *Arch Neurol*. 2007;64:1467–1477.
47. Khan UA, Liu L, Provenzano FA, et al. Molecular drivers and cortical spread of lateral entorhinal cortex dysfunction in preclinical Alzheimer's disease. *Nat Neurosci*. 2014;17:304–311.
48. Reuter M, Rosas HD, Fischl B. Highly accurate inverse consistent registration: a robust approach. *Neuroimage*. 2010;53:1181–1196.
49. Sawiak SJ, Wood NI, Williams GB, Morton AJ, Carpenter TA. Voxel-based morphometry in the R6/2 transgenic mouse reveals differences between genotypes not seen with manual 2D morphometry. *Neurobiol Dis*. 2009;33:20–27.
50. Gross MI, Demo SD, Dennison JB, et al. Antitumor activity of the glutaminase inhibitor CB-839 in triple-negative breast cancer. *Mol Cancer Ther*. 2014;13:890–901.
51. Schobel SA, Kelly MA, Corcoran CM, et al. Anterior hippocampal and orbitofrontal cortical structural brain abnormalities in association with cognitive deficits in schizophrenia. *Schizophr Res*. 2009;114:110–118.
52. Lewandowski NM, Small SA. Brain microarray: finding needles in molecular haystacks. *J Neurosci*. 2005;25:10341–10346.
53. van den Buuse M. Modeling the positive symptoms of schizophrenia in genetically modified mice: pharmacology and methodology aspects. *Schizophr Bull*. 2010;36:246–270.
54. Pedersen CS, Sørensen DB, Parachikova AI, Plath N. PCP-induced deficits in murine nest building activity: employment of an ethological rodent behavior to mimic negative-like symptoms of schizophrenia. *Behav Brain Res*. 2014;273:63–72.
55. Clifton NE, Morisot N, Girardon S, Millan MJ, Loiseau F. Enhancement of social novelty discrimination by positive allosteric modulators at metabotropic glutamate 5 receptors: adolescent administration prevents adult-onset deficits induced by neonatal treatment with phencyclidine. *Psychopharmacology (Berl)*. 2013;225:579–594.
56. Bissonette GB, Powell EM. Reversal learning and attentional set-shifting in mice. *Neuropharmacology*. 2012;62:1168–1174.
57. Pierson JL, Pullins SE, Quinn JJ. Dorsal hippocampus infusions of CNQX into the dentate gyrus disrupt expression of trace fear conditioning. *Hippocampus*. 2015;25:779–785.
58. Deacon RM. Assessing nest building in mice. *Nat Protoc*. 2006;1:1117–1119.

59. Maren S, Phan KL, Liberzon I. The contextual brain: implications for fear conditioning, extinction and psychopathology. *Nat Rev Neurosci*. 2013;14:417–428.
60. Eastwood SL, Harrison PJ. Decreased expression of vesicular glutamate transporter 1 and complexin II mRNAs in schizophrenia: further evidence for a synaptic pathology affecting glutamate neurons. *Schizophr Res*. 2005;73:159–172.
61. Poels EM, Kegeles LS, Kantrowitz JT, et al. Glutamatergic abnormalities in schizophrenia: a review of proton MRS findings. *Schizophr Res*. 2014;152:325–332.
62. Sawada K, Barr AM, Nakamura M, et al. Hippocampal complexin proteins and cognitive dysfunction in schizophrenia. *Arch Gen Psychiatry*. 2005;62:263–272.
63. Gilani AI, Chohan MO, Inan M, et al. Interneuron precursor transplants in adult hippocampus reverse psychosis-relevant features in a mouse model of hippocampal disinhibition. *Proc Natl Acad Sci U S A*. 2014;111:7450–7455.
64. Karlsson RM, Tanaka K, Heilig M, Holmes A. Loss of glial glutamate and aspartate transporter (excitatory amino acid transporter 1) causes locomotor hyperactivity and exaggerated responses to psychotomimetics: rescue by haloperidol and metabotropic glutamate 2/3 agonist. *Biol Psychiatry*. 2008;64:810–814.
65. Karlsson RM, Tanaka K, Saksida LM, Bussey TJ, Heilig M, Holmes A. Assessment of glutamate transporter GLAST (EAAT1)-deficient mice for phenotypes relevant to the negative and executive/cognitive symptoms of schizophrenia. *Neuropsychopharmacology*. 2009;34:1578–1589.
66. Turrigiano GG, Nelson SB. Hebb and homeostasis in neuronal plasticity. *Curr Opin Neurobiol*. 2000;10:358–364.
67. Campanac E, Debanne D. Spike timing-dependent plasticity: a learning rule for dendritic integration in rat CA1 pyramidal neurons. *J Physiol*. 2008;586:779–793.
68. Piskorowski RA, Nasrallah K, Diamantopoulou A, et al. Age-dependent specific changes in area CA2 of the hippocampus and social memory deficit in a mouse model of the 22q11.2 deletion syndrome. *Neuron*. 2016;89:163–176.
69. Giusti SA, Vercelli CA, Vogl AM, et al. Behavioral phenotyping of Nestin-Cre mice: implications for genetic mouse models of psychiatric disorders. *J Psychiatr Res*. 2014;55:87–95.
70. Forni PE, Scuoppo C, Imayoshi I, et al. High levels of Cre expression in neuronal progenitors cause defects in brain development leading to microencephaly and hydrocephaly. *J Neurosci*. 2006;26:9593–9602.
71. Bao X, Pal R, Hascup KN, et al. Transgenic expression of Glud1 (glutamate dehydrogenase 1) in neurons: in vivo model of enhanced glutamate release, altered synaptic plasticity, and selective neuronal vulnerability. *J Neurosci*. 2009;29:13929–13944.
72. Liu Z, Zhao W, Xu T, Pei D, Peng Y. Alterations of NMDA receptor subunits NR1, NR2A and NR2B mRNA expression and their relationship to apoptosis following transient forebrain ischemia. *Brain Res*. 2010;1361:133–139.
73. Bolkan SS, Carvalho Poyraz F, Kellendonk C. Using human brain imaging studies as a guide toward animal models of schizophrenia. *Neuroscience*. 2016;321:77–98.
74. Maziade M, Bissonnette L, Rouillard E, et al. 6p24-22 region and major psychoses in the Eastern Quebec population. Le Groupe IREP. *Am J Med Genet*. 1997;74:311–318.